Supplemental Information:
Global Kinetic Analysis of Mammalian E3 Reveals pH-dependent NAD^+/NADH Regulation, Physiological Kinetic Reversibility, and Catalytic Optimum

Michael A. Moxley[‡], Daniel A. Beard[‡,1], Jason N. Bazil[‡].
[‡]From the Department of Molecular and Integrative Physiology, University of Michigan, Ann Arbor, Michigan 48109
[*]Running title: Mammalian E3 pH-dependent Activation/Inhibition
[1]To whom correspondence should be addressed: Tel: 734-763-8040; E-mail:beardda@umich.edu

Fluorescence binding assay methodology

Fluorescence binding assays were analyzed by assuming the observed spectra are a linear combination of bound and unbound species as shown in Eqn. S1. The first observed spectrum, in the absence of titrant, is considered to be unbound, where the last observed spectrum is considered to represent the bound spectrum. This method, which has been fully described elsewhere (1), allows for the use of the entire spectrum in the analysis of spectroscopic binding data rather than the more narrow approach of selecting a single wavelength for analysis. In Eqn. S1, $S_{obs}(\lambda)_i$ and α_i represent the observed spectrum, as a function of wavelength (λ), and fraction of the ligand bound state at the i^{th} titration point, respectively. $S_{i=n}(\lambda)$ and $S_{i=0}(\lambda)$ represent the final and initial observed spectrum at the n^{th} and zeroth titration point, respectively.

$$S_{obs}(\lambda)_i = \alpha_i S(\lambda)_{i=n} + (1-\alpha_i) S(\lambda)_{i=0} \tag{S1}$$

The solution to Eqn. S1. is a linear least squares solution and is shown in Eqn. S2. The angled brackets denote difference, spectral vectors in λ, and are multiplied by taking their dot product.

$$\alpha(i) = \frac{\left\langle S(\lambda)_{i=n} - S(\lambda)_{i=0} \right\rangle \cdot \left\langle S_{obs}(\lambda)_i - S(\lambda)_{i=0} \right\rangle}{\left\langle S(\lambda)_{i=n} - S(\lambda)_{i=0} \right\rangle \cdot \left\langle S(\lambda)_{i=n} - S(\lambda)_{i=0} \right\rangle} \tag{S2}$$

Therefore, the above analysis provides a linear least squares fit to each spectrum at the i^{th} titration point, and a binding curve as a function of titrant (Fig. 2). The solved vector, α, is an estimation of the fractional occupancy of a ligand to a certain enzyme state, and thus can be incorporated into the global model fitting to account for the binding of a specific ligand to a specific state in a direct manner. Notably, the final observed spectrum in the titration does not exactly represent a 100 % bound spectrum, but is rather a close approximation. To account for this, a factor is placed in front of the fitted fractional occupancy expression, which allows a more accurate estimation of the equilibrium dissociation constant to be determined. This practice was also implemented in the original description of this method (1).

E3 FAD spectroscopic analysis

Pig heart E3 FAD absorption data (Fig. 4) were obtained using graph digitizing software (ScanIt 1.06 (amsterCHEM)) from Fig. 3 in (2) and Fig. 4 and 1 in (3), respectively. To obtain consistent integer wavelength values from the extracted literature spectra, the spectra were interpolated generally between 300 and 650 nm. This step was necessary to have consistent wavelengths within a spectral data set when applying a singular value decomposition or other mathematical operations that require wavelength consistency in the spectral vectors. For instance, a singular value decomposition was applied to the NAD^+ titration of $2e^-$ reduced pig heart E3 in Fig. 4A using MATLAB 2014b software.

Spectroscopic absorbance data are assumed to be a linear independent combination of species, as is assumed in the Beer-Lambert law (4). For instance, the spectral data shown in Fig. 4D can be grouped into a *m x n* matrix *A*, where *m* is the number of titrations and *n* is the number of wavelengths at which the data was collected. In this case, $m = 7$ and $n = 321$. The three major redox species, with known spectra, are shown in Fig. 4E and can be grouped into a *m x n* matrix *B*, with 3 species and 321 wavelengths. The 7 x 3 matrix *X* (Eqn. S3) contains three column vectors containing the concentrations of each of the three species at each titration point.

$$A \cdot X = B \tag{S3}$$

The solution to this problem can be found by taking the pseudoinverse ($(A^TA)^{-1}A^T$) of matrix *A* and multiplying by matrix *B*, shown in Eqn. S4.

$$X = \left(A^T \cdot A\right)^{-1} A^T B \tag{S4}$$

Each row of matrix *X* contains some amount of each major species and was normalized to give the fraction of redox species per titration point based on the total enzyme concentration. To avoid negative solutions, when concentrations are very small, we chose to use a non-negative linear least squares solver (lsqnonneg) using MATLAB 2014b software for the final result of this analysis. Overall, this solution, which was obtained using model free analysis (4), allows one to directly fit the extracted enzyme fractional states to a model.

To fit this result to a model, the dihydrolipoamide titration of E3 was simulated by numerically integrating (using ode15s in MATLAB 2014b) the model shown in Fig. 1A, which includes dihydrolipoamide, lipoamide, and the major enzyme redox states as state variables. Each amount of dihydrolipoamide added was allowed 10 min of simulation time; simulating each addition for longer times did not have an effect on the result. Optimization of the model parameters with this simulation were included with the rest of the data sets during the global fitting process.

Model fitting

Data were fitted using MATLAB 2014b software (The MathWorks, Natick, MA) using customized code of a simulated annealing algorithm and then further optimized using the local non-linear optimization function FMINCON. Importantly, data sets were fitted simultaneously, or globally, as compared to individual dataset fitting which is traditional in enzyme kinetic analysis (5).

Time-dependent experiments were simulated by numerically integrating the rate equations for A, B, P, and Q derived from the steady state solution (Solution to Eqn. S5). Numerical integration was carried out with ode45 (Runge-Kutta algorithm) in MATLAB and fitted simultaneously with initial rate data.

In order to simulate/fit the dihydrolipoamide titration (Fig. 4F), the model was numerically integrated using the full equations (ie. Right hand side of Eqn. S5 not equaled to zero) with ode15s in MATLAB 2014b. The state variables for this simulation included all substrates, products, and enzyme states. The data was fitted either allowing all equilibrium dissociation constants to be independent or dependent of the redox state of the enzyme; this approach was discussed previously (6). This added sophistication in the model was implemented to better simulate redox associated changes in enzyme ligand affinity.

In an effort to obtain the "best-fit", hundreds of fitting trials were conducted using the algorithms mentioned above with random initial starting points. However, attempts to fit all of the data together from random initial parameter values seemed to produce poor results. Therefore, we used a divide and conquer approach of fitting smaller subsets of the data– progressively building towards the complete data set.

When fitting progress curve or time dependent data, we found that these data sets produce a significant bottle neck in fitting trials due to the task of numerical integration. To speed up integration of the model, C-code matlab executable files were generated and ran on a HP Z820 workstation (linux OS) equipped with 8 cores (intel E5-2609 @2.40 GHz) and 32 GB RAM.

Best-fit parameter perturbation

To investigate the sensitivity of model simulations shown in Fig. 8 to the best-fit parameters, we randomly perturbed all of the best-fit parameters by randomly selecting parameter values within a 10% boundary of the original parameters in Table 1. We repeated this process 1000 times to obtain a large collection of randomly perturbed parameters from the best-fit. We then simulated all 1000 parameter sets for all collected data sets and have displayed the maximum and minimum simulations in Fig. S8 with the data. We used these 1000 parameter sets to then simulate (Fig. S9) the E3 mammalian flux surface and cross sections. In Fig. S9A and C, we show the maximum and minimum flux surfaces with the original surfaces produced from the global best-fit parameters. In Fig. S9B and D, we show all 1000 cross sections of the flux surfaces produced from the 1000 perturb parameter sets.

Progress curve approximation

Another strategy we used to better or more efficiently fit progress curve data involved approximating the rate of change of the progress curves, which change with time. We found this additional step in the fitting procedure to be especially helpful when trying to fit data sets that contain both pH-dependent NAD^+ activation and inhibition; as opposed to simply either NAD^+ activation or inhibition alone.

Progress curve rates were estimated by first fitting the progress curve data using cubic spline interpolation and then differentiating at these time points. The derivatives were then integrated using the cumulative trapezoidal numerical integration method, with given initial conditions, to arrive at calculated substrate and product concentrations at a particular time point. These concentrations are then used to calculate the rates using the flux expression at each time point.

The fitting procedure then minimizes the difference between the calculated derivatives and the computed rates at each time point using the flux expression and the optimized kinetic parameters. The advantage of this progress curve approximation method is that it avoids numerical integration during the actual fitting of the data and instead involves computing the flux at different time points, which is much less computationally intensive. Furthermore, it can provide better initial parameters for fitting progress curve data, relative to just fitting the initial rates as a preliminary fitting option.

3-state redox model fitting for pH-dependent activation/inhibition data

In one approach we started from 21 parameter sets (using a local optimizer; Supplement) that fit the human liver E3 data, in the most accurate manner (See (6)), but arrived at fits that did not accurately simulate the forward E3 reaction as a function of pH (Fig. 5C; dashed line). We also started from random initial parameter values (using both global and local optimization methods), but arrived at the same result

as the former approach. A method, described in the Supplement (See progress curve approximation above), to fit progress curve data using time-dependent rates was also implemented, but also failed to fit the data. We conclude that it is not possible to accurately fit the data set in Fig. 5 using the previously described 3-state redox model (6) (Fig. 5; dashed lines).

pH-dependent E3 flux optimization

-pH as an adjustable parameter

Optimizations were implemented using simulated annealing followed by local minimization with NAD^+/NADH, Lipo/DHL, and pH as adjustable parameters. In this optimization routine, the best of 1000 attempts were used for the displayed results (Table 2). These results are plotted in Fig. 11 and 12. The parameter bounds for NAD^+/NADH and Lipo/DHL were 10^{12} and 10^{-12} for upper and lower bound, respectively. The pH was bound between 4 and 9.

-pH fixed at different values

Optimizations were carried out with a simulated annealing algorithm, followed by a local minimizer, treating the NAD^+/NADH and Lipo/DHL ratios as adjustable parameters at different fixed pH values. Thus, 13 separate optimizations were carried out for each pH value (Fig. 13). Furthermore, 50 attempts were made at each pH value to obtain the most optimum reverse flux for both mammalian and *E. coli* E3. This routine, thus, produced 650 separate optimizations a piece for both mammalian and *E. coli* E3. The same protocol was also implemented to optimize mammalian and *E. coli* E3 forward flux (Fig. 14). The NAD^+/NADH ratio was given the upper bounds of 10^2 (Ec-E3) and 25 (mam-E3), and lower bounds of 10^{-2} (Ec-E3) and 25^{-1} (mam-E3). The Lipo/DHL ratio was given the upper and lower bound of 10^{12} and 10^{-12}, respectively, for both Ec-E3 and mam-E3.

$$\begin{bmatrix} -\left(f_{A_1}k_1 + f_{Q_1}k_6[H^+]\right) & f_{H^+}f_{P_2}k_2 & f_{B_3}k_5 & 0 \\ f_{A_1}k_1 & -\left(f_{H^+}f_{P_2}k_2 + f_{H^+}f_{Q_2}k_7[H^+] + f_{H^+}k_3\right) & k_4 & f_{B_4}k_8 \\ f_{Q_1}k_6[H^+] & f_{H^+}k_3 & -\left(k_4 + f_{A_3}k_{10} + f_{B_3}k_5\right) & f_{P_4}k_9 \\ 0 & f_{H^+}f_{Q_2}k_7[H^+] & f_{A_3}k_{10} & -\left(f_{P_4}k_9 + f_{B_4}k_8\right) \\ 1 & 1 & 1 & 1 \end{bmatrix} \begin{bmatrix} S_1 \\ S_2 \\ S_3 \\ S_4 \end{bmatrix} = \begin{bmatrix} 0 \\ 0 \\ 0 \\ 0 \\ Et \end{bmatrix} \quad \text{(S5)}$$

Equation matrix for a 4-state redox steady-state model. In this model, E3 is composed of the oxidized (S_1), $2e^-$ disulfide reduced (S_2), $2e^-$ FAD reduced (S_3), and both $2e^-$ disulfide and $2e^-$ FAD reduced (S_4) states (Fig. 1A). The final row in the matrix accounts for the total enzyme concentration (E_t), which is the sum of all enzyme states. An analytical solution for this kinetic model was determined by performing a pseudoinverse on the equation matrix using MATLAB 2014b symbolic toolbox.

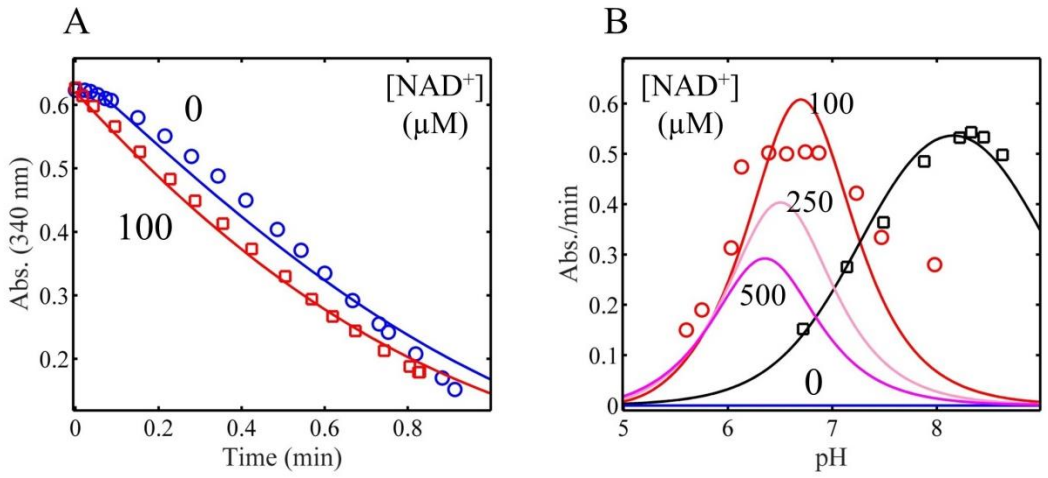

Figure S1. Human liver E3 kinetic data with 3-state redox kinetic model simulations. A) Human liver E3 reverse reaction progress curve data at pH 6.5 obtained from (7), with no initially added NAD^+ (blue circles) and 100 μM NAD^+ (red squares) with simulations (solid lines) to a 3-state redox kinetic model using best-fit parameters obtained from Table 1 in (6) under the Human liver E3 heading. B) Human liver E3 reverse (red circles) and forward (black squares) initial velocity data at pH 6.5 and 8.5 respectively, obtained from (7), and corresponding simulations are shown with red and black lines, respectively, using the same parameters used to simulate progress curves in (A). The reverse initial velocity data (red circles) contained 100 μM NADH and NAD^+. Additional simulations using the same parameters were generated with 0 (blue line), 250 (light pink), and 500 (dark pink) μM NAD^+.

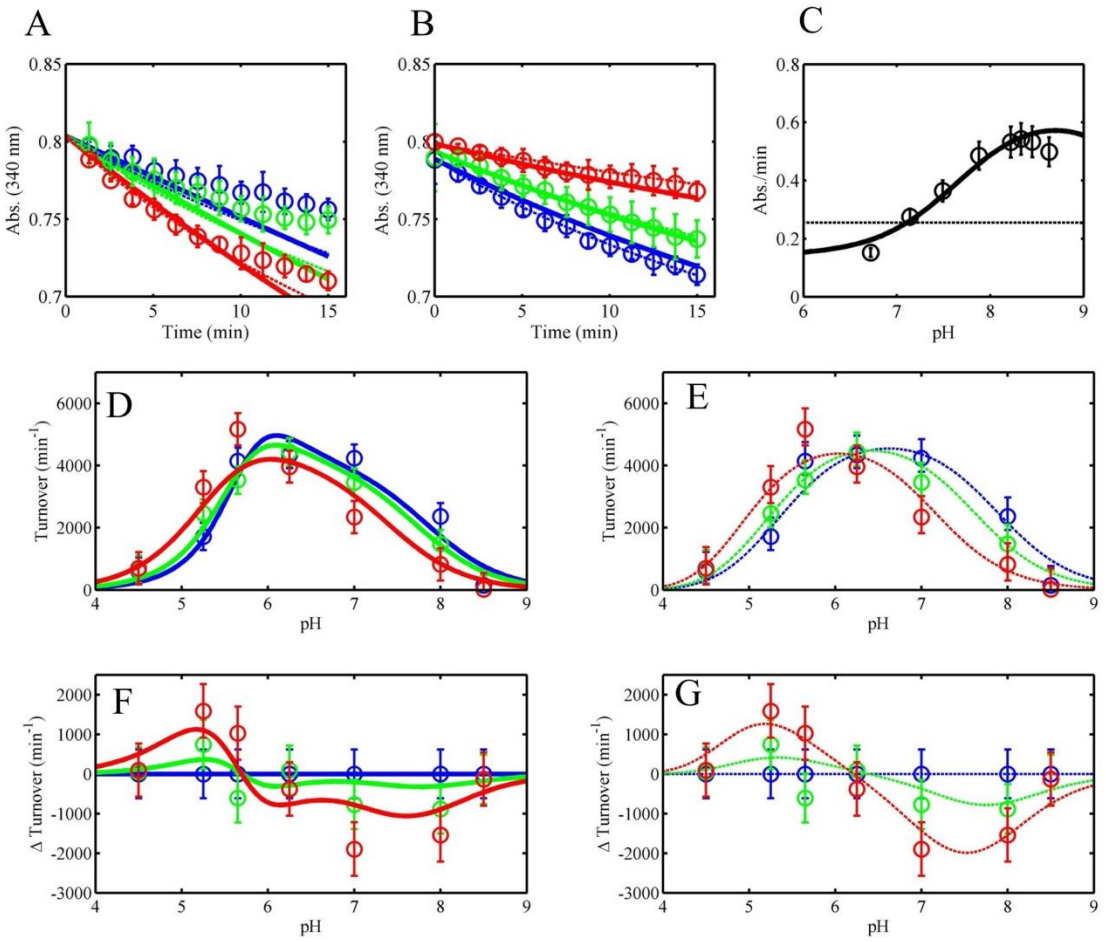

Figure S2. Mammalian E3 pH-dependent NAD^+ activation/inhibition fitted to a 4 and 3-state redox independent K_d model. A) Pig heart E3 reverse reaction progress curves in acidic conditions (pH = 5.25) in different initially added amounts of NAD^+ (0, 100, 500 µM), shown as blue, green, and red circles respectively. Model simulations are shown as dashed (3-state model) and solid (4-state model) lines of the corresponding data marker color. B) Pig heart E3 reverse reaction progress curves in basic conditions (pH = 8) in different initially added amounts of NAD^+ (0, 100, 500 µM), shown as blue, green, and red circles respectively. Model simulations are shown as dashed (3-state model) and solid (4-state model) lines of the corresponding data marker color. C) Human liver E3 pH-dependent forward initial rates (black circles) taken from Fig. 5 of (7). Model simulations are shown as black dashed (3-state model) and solid (4-state model) lines. D) Pig heart E3 pH-dependent reverse initial rates in different initially added amounts of NAD^+ (0, 100, 500 µM), shown as blue, green, and red circles respectively. (D) Model simulations are shown as solid (4-state model) lines of the corresponding data marker color. (E) Model simulations are shown as dashed (3-state model) lines of the corresponding data marker color. F) Difference plot (observed turnover (NAD^+ added)-observed turnover(no NAD^+)) of data and simulations shown in (D). G) Difference plot (observed turnover (NAD^+ added)-observed turnover(no NAD^+)) of data and simulation shown in (E). In panels A-E error bars represent standard deviations of the data from at least three experimental repeats, where error bars in panels F and G represent the propagation of error from the difference of the observed rates.

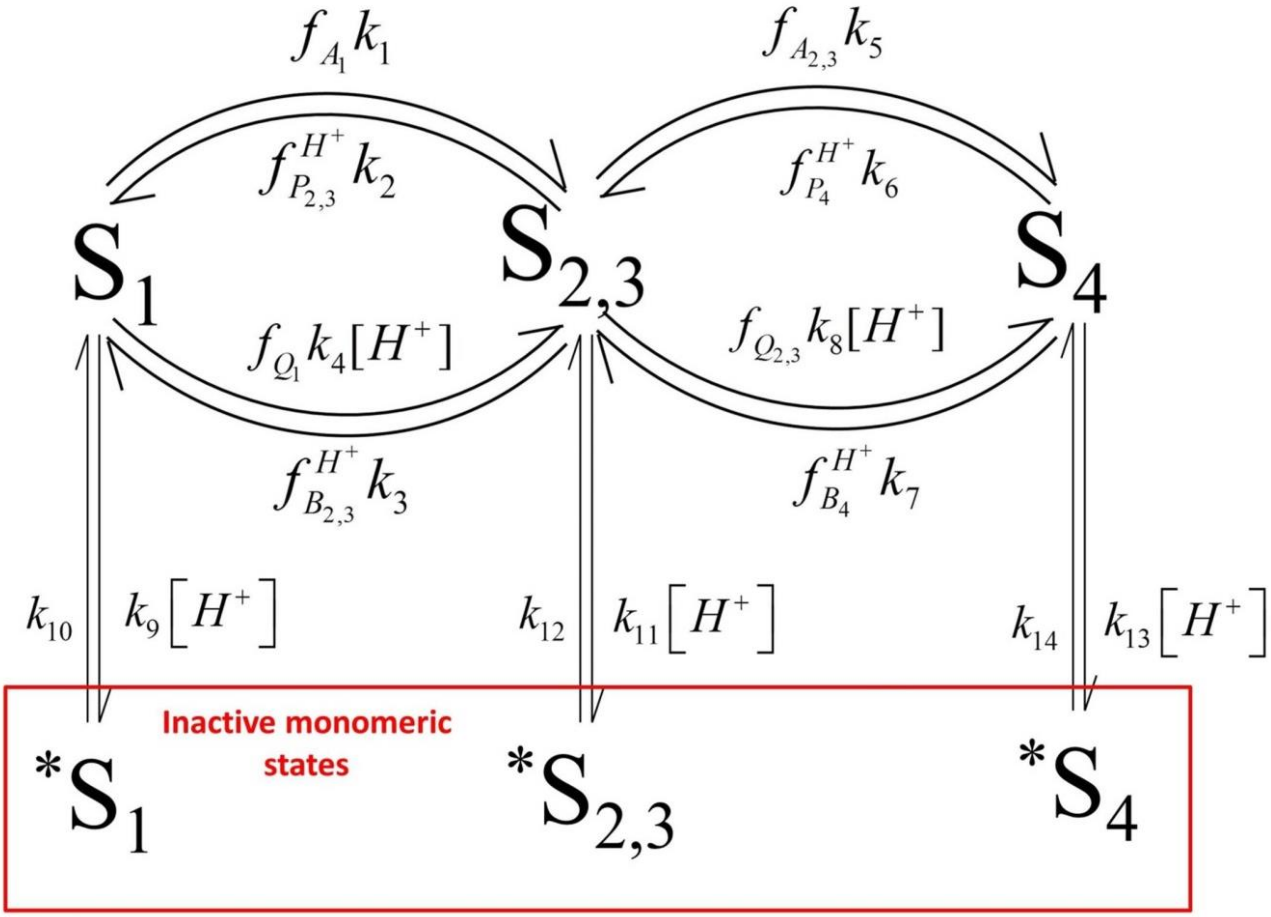

Figure S3. Mammalian E3 pH-dependent oligomeric state model. Enzyme oxidized, $2e^-$, and $4e^-$ reduced redox states are represented by S_1, $S_{2,3}$, and S_4, respectively (6). These states are considered to be active oligomeric states, which may represent dimer, tetramer, or perhaps a higher oligomeric state (8). Enzyme states that have an asterisk represent inactive monomeric states. This model was constructed based on pig heart E3 oligomeric state changes as a function of pH observed in (8).

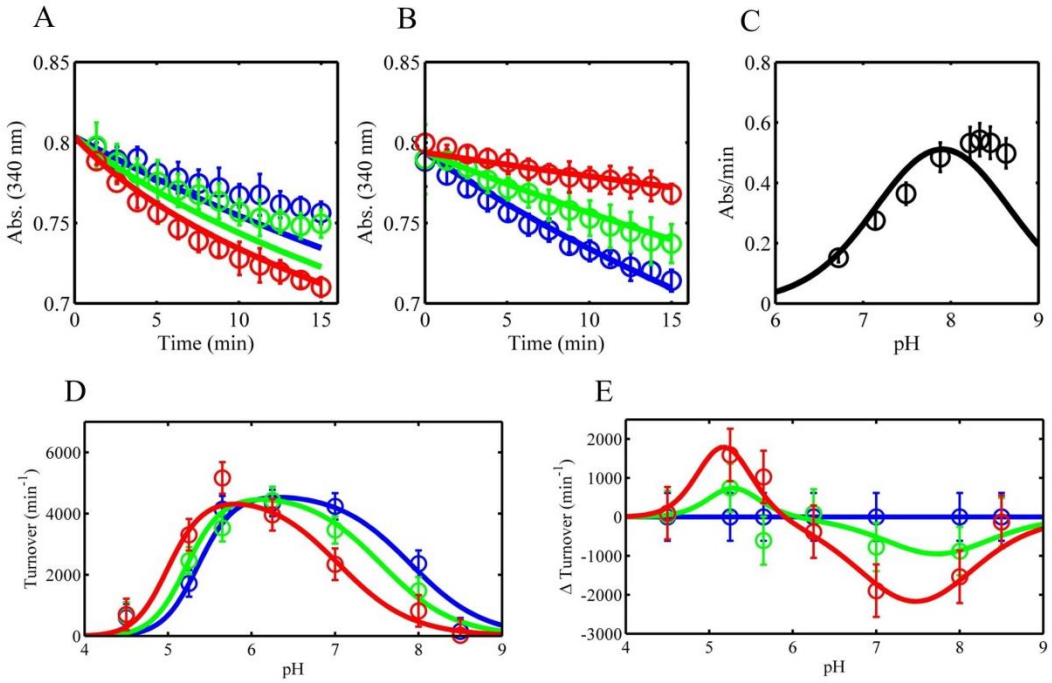

Figure S4. Mammalian E3 pH-dependent NAD^+ activation/inhibition fitted to a pH-dependent oligomeric state model described in Fig. S3. A) Pig heart E3 reverse reaction progress curves in acidic conditions (pH = 5.25) in different initially added amounts of NAD^+ (0, 100, 500 µM), shown as blue, green, and red circles respectively; simulations are represented by lines. B) Pig heart E3 reverse reaction progress curves in basic conditions (pH = 8) in different initially added amounts of NAD^+ (0, 100, 500 µM), shown as blue, green, and red circles respectively; simulations are represented by lines. C) Human liver E3 pH-dependent forward initial rates (black circles) taken from Fig. 5 of (7), with simulation shown as a black line. D) Pig heart E3 pH-dependent reverse initial rates in different initially added amounts of NAD^+ (0, 100, 500 µM), shown as blue, green, and red circles respectively; simulations are represented by lines. E) Difference plot (observed turnover(NAD^+ added)-observed turnover(no NAD^+)) of data (circles) and simulations (lines) with NAD^+ (0, 100, 500 µM), shown as blue, green, and red circles respectively. In panels A, B, and D error bars represent standard deviations of the data from at least three experimental repeats, while error bars in panel E represent the propagation of error from the difference of the observed rates. Error bars in panel C represent a 10% deviation from the data collected from Fig. 5 in (7).

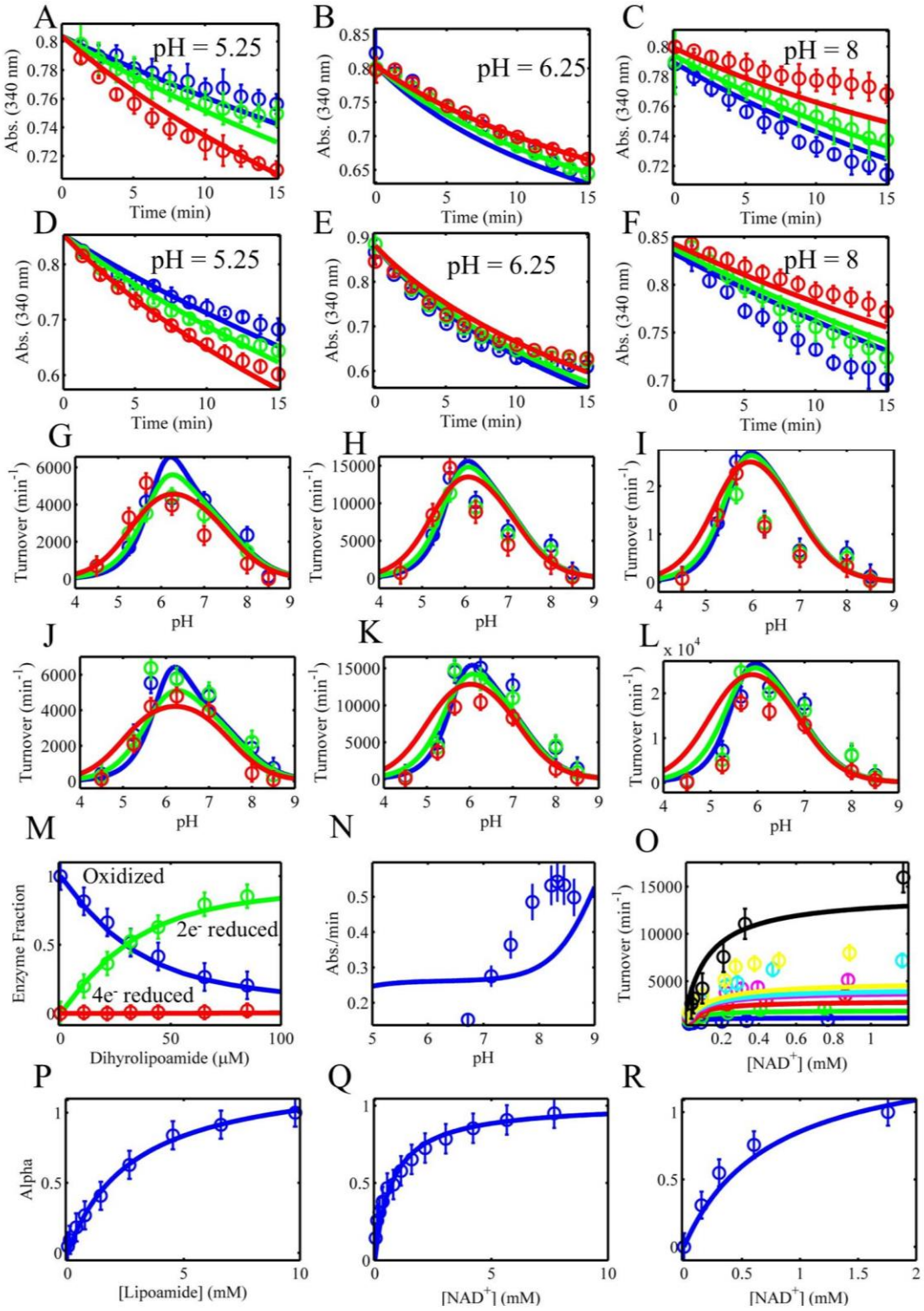

Figure S5. Global fitting of Mammalian E3 progress curve, reverse/forward initial velocity, and equilibrium titration data to a 4-state redox model with redox independent equilibrium dissociation constants. A-F) Pig heart E3 reverse reaction progress curve data were collected in different initially added amounts of NAD^+ (0, 100, 500 μM), shown as blue, green, and red circles respectively. Model simulations (4-state model) are shown as solid lines of the corresponding data marker color. All time

dependent assays shown in (A-F) contained 500 μM of initially added NADH. Panels (A-C) and (D-F) contained 0.25 and 1 mM DL-lipoamide, respectively. pH was held fixed at 5.25, 6.25, and 8 shown in panels (A-C) and (D-F), respectively. G-L) Pig heart E3 pH-dependent reverse initial velocity data were collected in different initially added amounts of NAD^+ (0, 100, 500 μM), shown as blue, green, and red circles, respectively. Error bars represent standard deviations of the data from at least three experimental repeats. Model simulations (4-state model) are shown as solid lines of the corresponding data marker color. Initial rates shown in panels (G-I) were obtained in 500 μM initially added NADH and 0.25 (G), 1 (H), and 3 mM (I) DL-Lipoamide. Initial rates shown in panels (J-L) were obtained with 250 μM initially added NADH and 0.25 (J), 1 (K), and 3 mM (L) DL-Lipoamide. M) Pig heart E3 fractional redox states were obtained from the dihyrolipoamide equilibrium titration shown in Figure 4D-F. The oxidized, $2e^-$ reduced, and $4e^-$ reduced states as a function of dihydrolipoamide are shown as blue, green, and red circles, respectively. N) Human liver E3 forward initial rate data as a function of pH was obtained from Fig. 5 of (7), and fitted along all other datasets in this figure. O) Forward initial rate data (circles) as a function of NAD^+ in different fixed concentrations of dihydrolipoamide (25 (blue), 40 (green), 50 (red), 100 (magenta), 250 (cyan), 500 (yellow), and 750 μM (black)), were taken from the top of Fig. 1 in (9), and simulated (lines) with globally fitted parameters along with all other datasets shown in this figure. P-R) Alpha values (blue circles) obtained from Figures 2C, 3C, and 4C were simulated (blue lines) with globally fitted parameters assuming rapid equilibrium binding of each ligand described by their corresponding enzyme state fractional occupancies (Eqn. 4). Error bars represent standard deviations of the data from at least three experimental repeats, while all literature derived data sets (panels M, N, and O) were assigned a 10% error according to the maximum ordinate value.

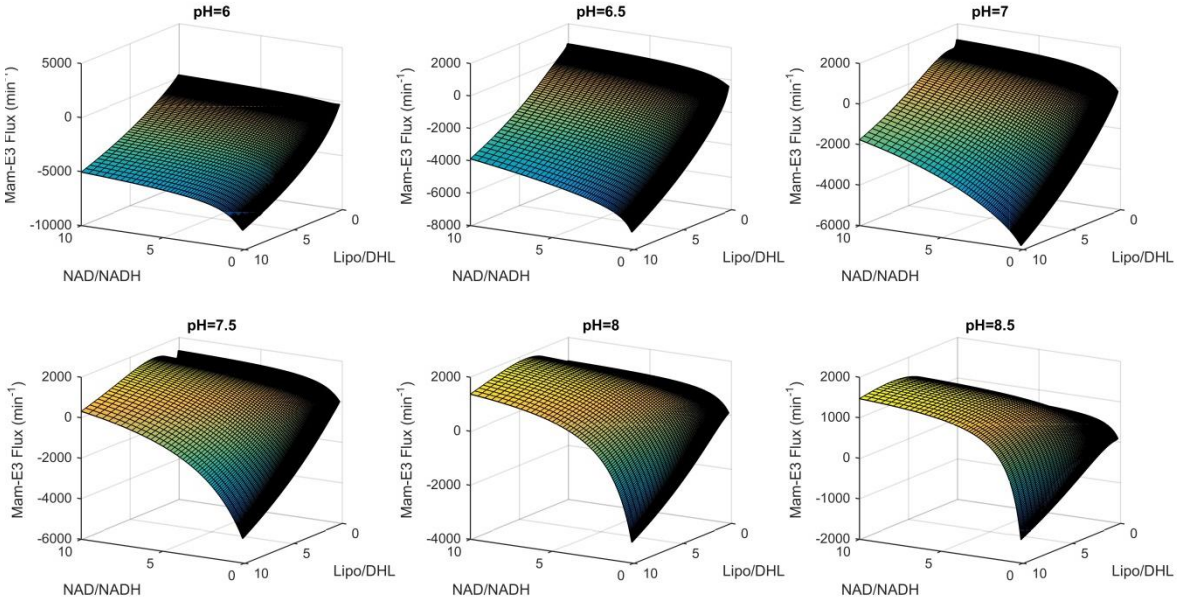

Figure S6. Calculated mammalian E3 NAD^+/NADH and Lipo/DHL flux surfaces as a function of pH. The globally fitted parameters (Table 1) obtained by fitting the data in Fig. 6, to the 4-state redox model, were used to calculate the mammalian E3 NAD^+/NADH and Lipo/DHL flux surfaces as a function of pH. In all panels, the forward and reverse fluxes are defined as being positive and negative, respectively. The forward flux is defined from left to right in Eqn. 2 in the main text.

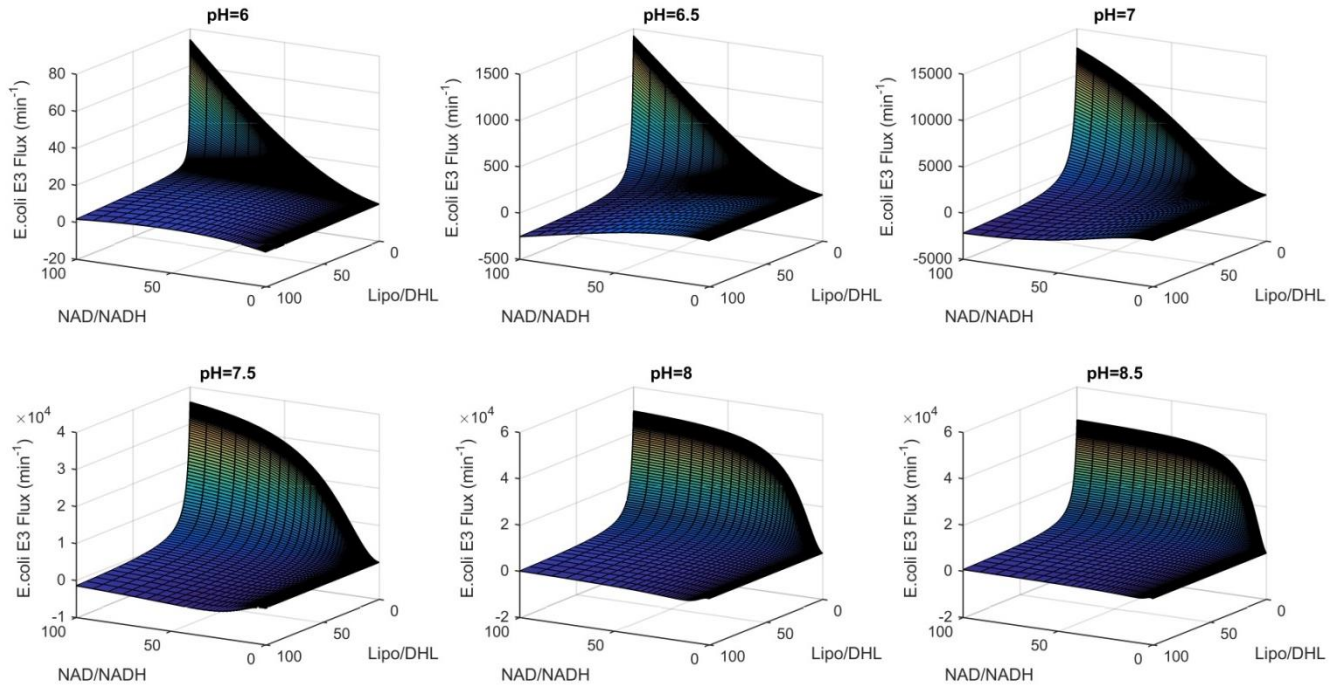

Figure S7. Calculated *E. coli* E3 NAD^+/NADH and Lipo/DHL flux surfaces as a function of pH. The globally fitted parameters obtained from Moxley et al. (6), to the 3-state redox-dependent K_d model, were used to calculate the *E. coli* E3 NAD^+/NADH and Lipo/DHL flux surfaces as a function of pH. In all panels, the forward and reverse fluxes are defined as being positive and negative, respectively. The forward flux is defined from left to right in Eqn. 2 in the main text.

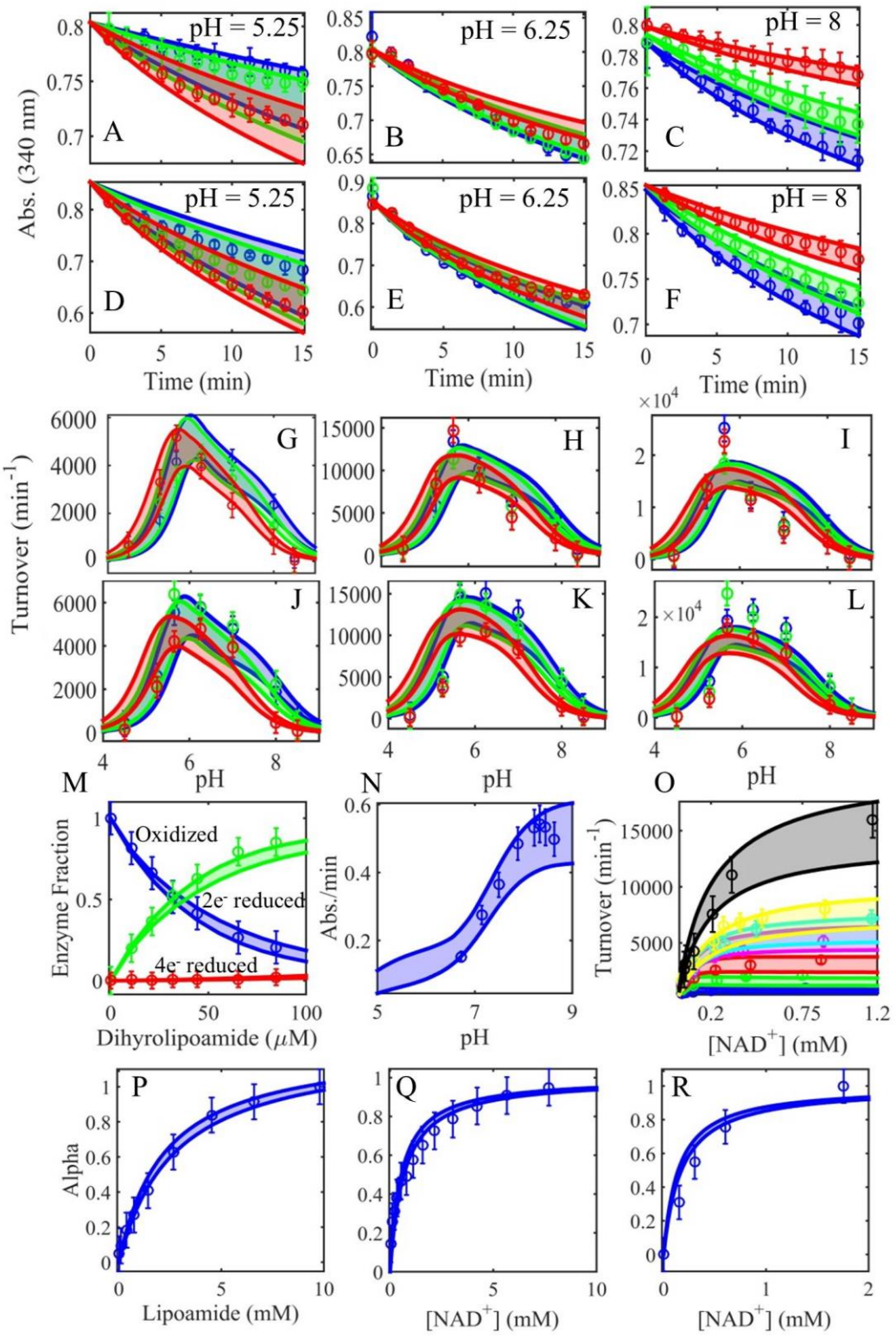

Figure S8. Simulation of prediction boundaries from random perturbations of best-fit parameter set. The original best-fit parameter set (Table 1) was perturbed by randomly adjusting all parameters within a 10% boundary of the original values. One-thousand parameter sets were generated and the maximum and minimum output of all 1000 parameter sets were used to create simulation prediction boundaries. Model

simulations (4-state model) of maximum and minimum output are shown as solid lines of the corresponding data marker color with shaded area in-between. A-F) Pig heart E3 reverse reaction progress curve data were collected in different initially added amounts of NAD^+ (0, 100, 500 μM), shown as blue, green, and red circles respectively. All time dependent assays shown in (A-F) contained 500 μM of initially added NADH. Panels (A-C) and (D-F) contained 0.25 and 1 mM DL-lipoamide, respectively. pH was held fixed at 5.25, 6.25, and 8 shown in panels (A-C) and (D-F), respectively. G-L) Pig heart E3 pH-dependent reverse initial velocity data were collected in different initially added amounts of NAD^+ (0, 100, 500 μM), shown as blue, green, and red circles, respectively. Error bars represent standard deviations of the data from at least three experimental repeats. Model simulations (4-state model) are shown as solid lines of the corresponding data marker color. Initial rates shown in panels (G-I) were obtained in 500 μM initially added NADH and 0.25 (G), 1 (H), and 3 mM (I) DL-Lipoamide. Initial rates shown in panels (J-L) were obtained with 250 μM initially added NADH and 0.25 (J), 1 (K), and 3 mM (L) DL-Lipoamide. M) Pig heart E3 fractional redox states were obtained from the dihyrolipoamide equilibrium titration shown in Figure 4D-F. The oxidized, $2e^-$ reduced, and $4e^-$ reduced states as a function of dihydrolipoamide are shown as blue, green, and red circles, respectively. N) Human liver E3 forward initial rate data as a function of pH was obtained from Fig. 5 of (7), and fitted along all other datasets in this figure. O) Forward initial rate data (circles) as a function of NAD^+ in different fixed concentrations of dihydrolipoamide (25 (blue), 40 (green), 50 (red), 100 (magenta), 250 (cyan), 500 (yellow), and 750 μM (black)), were taken from the top of Fig. 1 in (9), and simulation (lines) along with all other datasets shown in this figure. P-R) Alpha values (blue circles) obtained from Figures 2C, 3C, and 4C and simulations are shown as solid lines. Error bars represent standard deviations of the data from at least three experimental repeats, while all literature derived data sets (panels M, N, and O) were assigned a 10% error according to the maximum ordinate value.

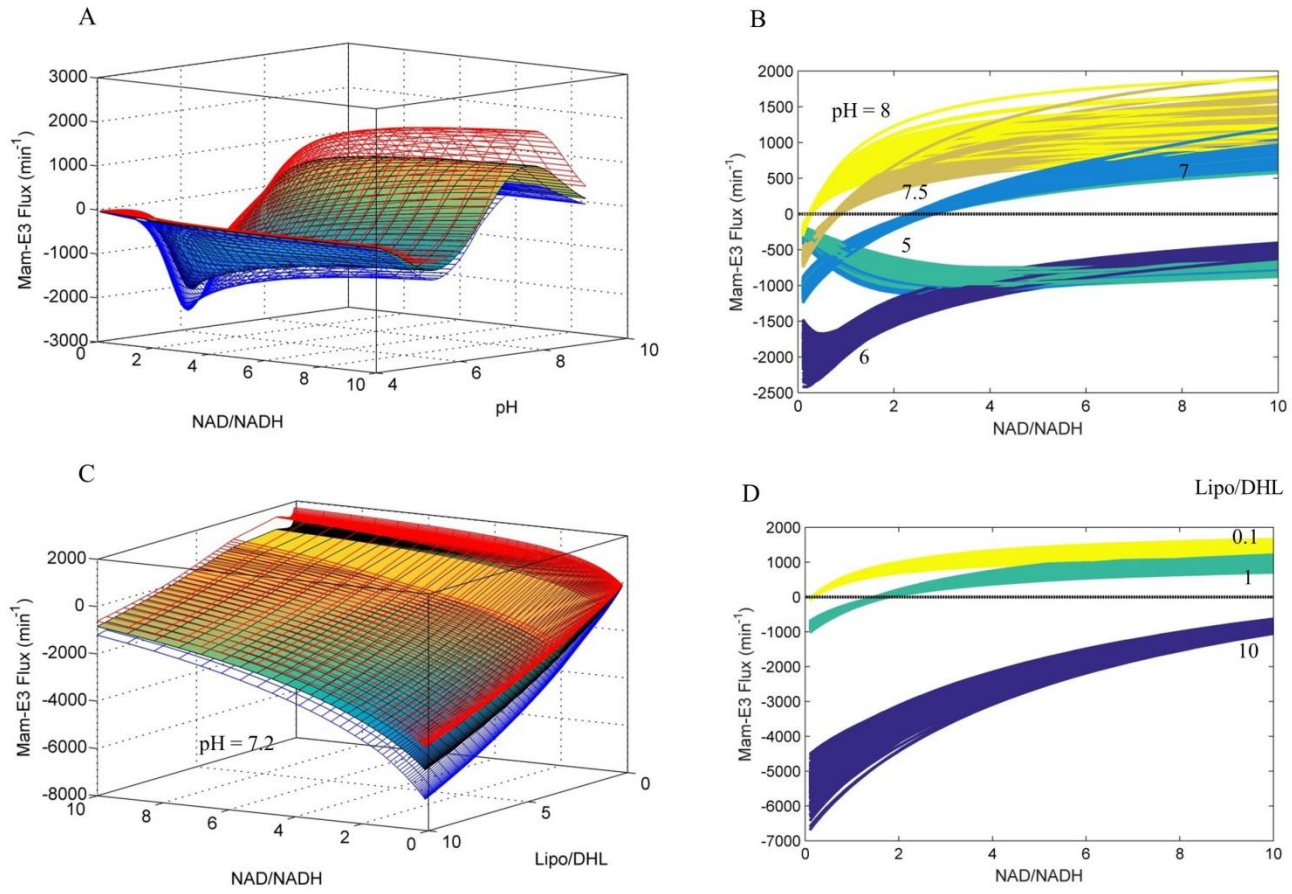

Figure S9. Calculated mammalian E3 NAD^+/NADH, Lipo/DHL, and pH-dependent flux surface with randomly perturbed best-fit parameters. The globally fitted parameters (Table 1) obtained by fitting the data in Fig. 6, to the 4-state redox model, were randomly perturbed with a 10% upper and lower bound from the original parameter set. This process was repeated to yield 1000 parameter sets. A) Mam-E3 flux as a function of NAD^+/NADH and pH, at a constant Lipo/DHL ratio of 1, were used to calculate the mammalian E3 flux surface for all 1000 parameter sets. The maximum (red mesh) and minimum (blue mesh) flux from these calculations are shown along with the original surface calculated using the best-fit global parameters. B) E3 flux(NAD^+/NADH, pH, Lipo/DHL = 1) cross sections at pH 5, 6, 7, 7.5, and 8 of 1000 parameter sets derived from perturbations of the original best-fit parameter set. The black line is a reference for zero flux. C) E3 flux as a function of NAD^+/NADH and Lipo/DHL, at a constant pH of 7.2, were used to calculate the mam-E3 flux surface for the 1000 parameter sets. The maximum (red mesh) and minimum (blue mesh) flux from these calculations are shown along with the original surface calculated using the best-fit global parameters. D) E3 flux(NAD^+/NADH, pH = 7.2, Lipo/DHL) cross sections at Lipo/DHL ratios of 0.1, 1, and 10 of 1000 parameter sets derived from perturbations of the original best-fit parameter set. The black line is a reference for zero flux. In all panels, the forward and

reverse fluxes are defined as being positive and negative, respectively. The forward flux is defined from left to right in Eqn. 2.

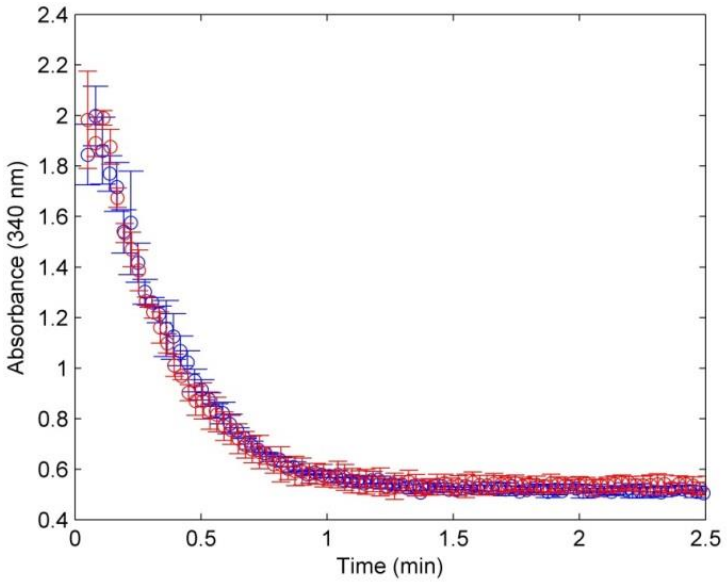

Figure S10. Progress curves using 50 mM Tris (blue) and MOPS (red) at pH 8 in 250 µM NADH, 3 mM DL-lipoamide, 0.3 mM EDTA, 0.67 mg/ml BSA, and 0.2 µM pig heart E3 at 25 °C. Duplicate assays were averaged and error bars represent standard deviations.

Lipoamide stereochemistry and kinetic modeling

The natural conformation of lipoamide is the R enantiomer (D-Lipoamide) (10). We were unable however, to find a commercially available source for R-Lipoamide. Therefore, we have used a D/L lipoamide mixture. Although, we investigated whether accounting for the fact that another isomer of lipoamide is present in the lipoamide mixture would better fit our pH-dependent initial velocity data.

Notably, S-Lipoic acid (not S-Lipoamide) has been shown to be an inhibitor (11), but we have not found any reports of S-Lipoamide (L-Lipoamide) as an inhibitor. Interestingly, we have found a report of the k_{cat}/K_m for DL-Lipoamide being about 30 times higher than R-Lipoic acid demonstrating that R-Lipoic acid is not a better substrate than DL-Lipoamide (See Table 1 of (11)). We do not know to what extent the lipoamide is in the D or L form, which creates a problem in accounting for the possible inhibition of L-lipoamide in our kinetic model. We also do not know how conditions such as concentration or pH affect D, L-lipoamide isomerization. Despite this, we have outlined a few strategies that account for the DL-lipoamide mixture in the model in an attempt to better fit pH-dependent initial velocity data.

In our view there are 3 ways to treat this issue:

1) Consider L-lipoamide as an inert component of the DL-lipoamide mixture, so that the true concentration of substrate (D-lipoamide) is less than the concentration of the known DL-lipoamide concentration. Without knowledge of the mixture, we can simply fit concentration of D-lipoamide with an upper bound being the DL-lipoamide concentration. This strategy did not improve fitting of the data, however.

2) Consider L-lipoamide as an inhibitor of the reaction. That is, we distinguish between D and L-lipoamide in the model by giving them separate dissociation constants for each redox state, but L-lipoamide is not considered to be a substrate; therefore, it does not turnover the enzyme. Here, we also needed to fit the percentage of the correct enantiomer relative to the total DL-lipoamide concentration, since as mention above we do not know this information. This strategy was used to try and fit the initial velocity data but did not improve the fitting (See Figure S11).

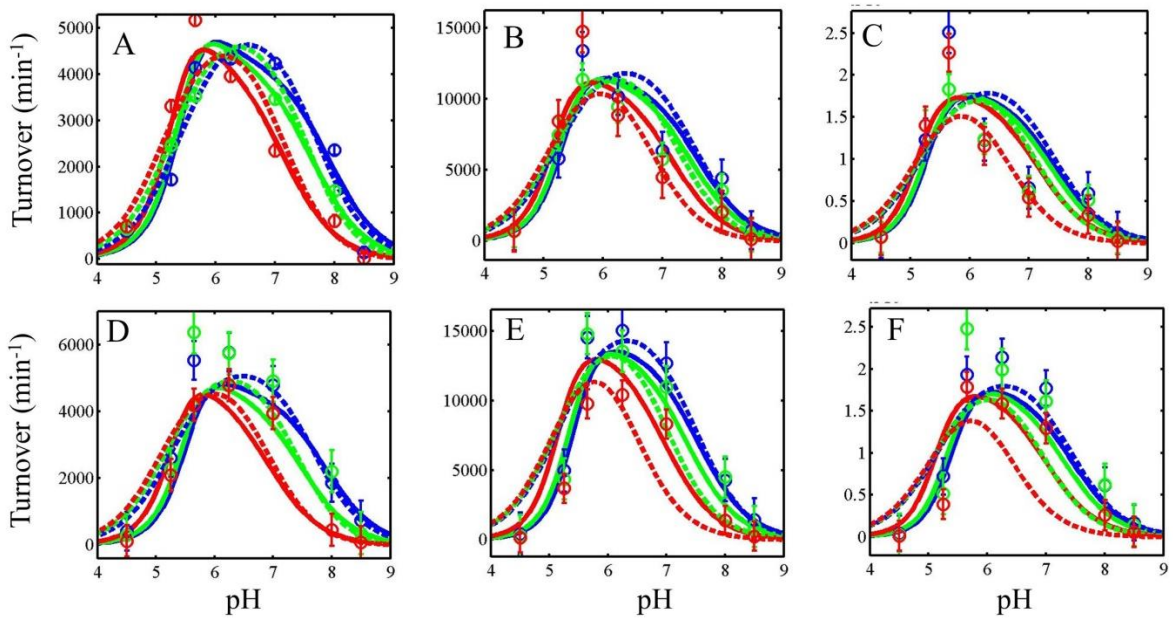

Figure S11. Comparison of initial velocity fitting between a 4-state redox K_d dependent model that differentiates between D and L-lipoamide (dashed lines) and the original model (solid line) that does not distinguish this condition. The model that distinguishes between lipoamide enantiomers imposes the condition that [DL-lipoamide] = [D-Lipoamide] + [L-lipoamide], where [DL-lipoamide] is known, and the proportions of the DL-Lipoamide mixture is a globally fitted parameter. The conditions for each panel are the same as in main text Figure 6 panels G-L. Panels A-C contained 500 µM NADH, with panels A, B, and C each with 0.25, 1, and 3 mM DL-lipoamide, respectively. Panels D-F contained 250 µM NADH, with panels D, E, and F each with 0.25, 1, and 3 mM DL-lipoamide, respectively.

In another attempt to fit these data better using strategy 2, we allowed the DL-lipoamide mixture to vary based on the total DL-lipoamide concentration. Although this may not have much chemical reasoning behind it, we were simply trying to improve the fit to the data. The result, shown in Figure S12 below, shows that allowing for this additional possibility did not improve the fitting.

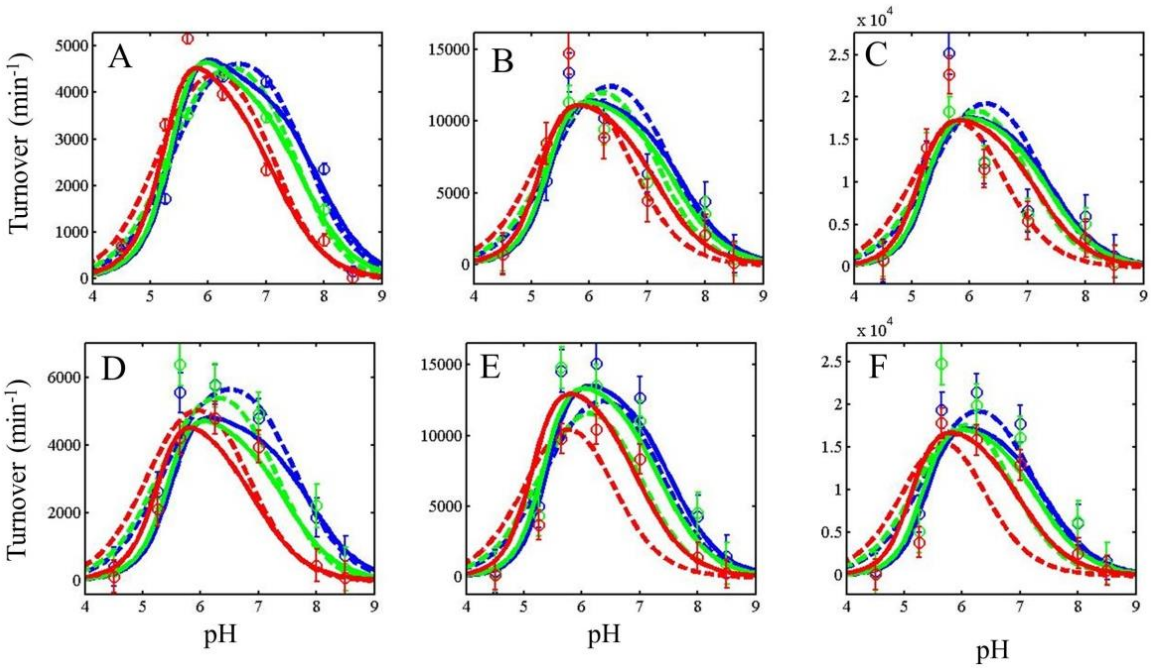

Figure S12. Comparison of initial velocity fitting between a 4-state redox K_d dependent model that differentiates between D and L-lipoamide (dashed lines) and the original model (solid line) that does not distinguish this condition. Additionally the stereochemically detailed model (dashed line) allows for the DL-lipoamide mixture to change as a function of DL-lipoamide total concentration. The model that distinguishes between lipoamide enantiomers imposes the condition that [DL-lipoamide] = [D-Lipoamide] + [L-lipoamide], where [DL-lipoamide] is known, [L-lipoamide] is a fitted parameter, and D-lipoamide is solved for based on the above mass balance equation. The DL-Lipoamide mixture is a fitted parameter. The conditions for each panel are the same as in main Figure 6 panels G-L. Panels A-C have 500 µM NADH, with panels A, B, and C each with 0.25, 1, and 3 mM DL-lipoamide. Panels D-F have 250 µM NADH, with panels D, E, and F each with 0.25, 1, and 3 mM DL-lipoamide.

Another assumption may be that the DL-lipoamide mixture can change with pH, but this would require a formidable change to the model, in which we have no data to support this mechanism.

3) Treating L-lipoamide as an alternative substrate: It is also very feasible that L-lipoamide is being consumed but at a lesser rate. Kinetic data with both human (11) and pig heart (10) E3 using L-lipoic acid shows that this enantiomer still turns over but at a slower rate (~ 20 fold lower k_{cat}/K_m) than the R-enantiomer. This leads us to believe that L-lipoamide is also a substrate and not just a putative inhibitor. This notion is also supported by a molecular docking study (12) that demonstrates only a 1.4 Å deviation between the reactive thiol of S-lipoamide relative to R-lipoamide. While this discrepancy in distance is certainly significant to distinguish between these substrates in catalytic reactivity, it demonstrates considerable probability that E3 can use S-lipoamide as a substrate. If this is true, L-lipoamide should be more appropriately modeled as an alternative substrate rather than a purely competitive dead-end inhibitor. However, accounting for these facts requires a substantial increase in the number of adjustable parameters for the model and there is insufficient data to statistically support a more expansive model as the model fits currently stand.

SUPPLEMENTAL REFERENCES

1. Duggleby, R. G., and Northrop, D. B. (1989) *Experientia* **45**, 87-92
2. Matthews, R. G., Ballou, D. P., and Williams, C. H., Jr. (1979) *J Biol Chem* **254**, 4974-4981
3. Matthews, R. G., and Williams, C. H., Jr. (1976) *J Biol Chem* **251**, 3956-3964
4. Maeder, M., and Neuhold, Y.-M. (2007) *Practical data analysis in chemistry*, Elsevier, Amsterdam ; London
5. Motulsky, H., and Christopoulos, A. (2004) *Fitting models to biological data using linear and nonlinear regression : a practical guide to curve fitting*, Oxford University Press, Oxford ; New York
6. Moxley, M. A., Beard, D. A., and Bazil, J. N. (2014) *Biophys J* **107**, 2993-3007
7. Ide, S., Hayakawa, T., Okabe, K., and Koike, M. (1967) *J Biol Chem* **242**, 54-60
8. Klyachko, N. L., Shchedrina, V. A., Efimov, A. V., Kazakov, S. V., Gazaryan, I. G., Kristal, B. S., and Brown, A. M. (2005) *J Biol Chem* **280**, 16106-16114
9. Tsai, C. S. (1980) *Int J Biochem* **11**, 407-413
10. Loffelhardt, S., Bonaventura, C., Locher, M., Borbe, H. O., and Bisswanger, H. (1995) *Biochem Pharmacol* **50**, 637-646
11. Hong, Y. S., Jacobia, S. J., Packer, L., and Patel, M. S. (1999) *Free Radic Biol Med* **26**, 685-694
12. Raddatz, G., and Bisswanger, H. (1997) *J Biotechnol* **58**, 89-100